JM PAPERS

On the maximum spreading of viscous droplets impacting flat solid surfaces

Lihui Liu[1] , Guobiao Cai[2], Weizong Wang[2] , Bijiao He[2] and Peichun Amy Tsai[1]

[1]Mechanical Engineering, University of Alberta, Edmonton, AB T6G 1H9, Canada
[2]School of Astronautics, Beihang University, Beijing 100191, PR China
Corresponding authors: Peichun Amy Tsai, peichun.amy.tsai@ualberta.ca; Bijiao He, hbj@buaa.edu.cn

We experimentally and theoretically examine the maximum spreading of viscous droplets impacting ultra-smooth solid surfaces, where viscosity plays a dominant role in governing droplet spreading. For low-viscosity droplets, viscous dissipation occurs mainly in a thin boundary layer near the liquid–solid interface, whereas for high-viscosity droplets, dissipation is expected to extend throughout the droplet bulk. Incorporating these dissipation mechanisms with energy conservation principles, two distinct theoretical scaling laws for the maximum spreading factor (β_m) are derived: $\beta_m \sim (We/Oh)^{1/6}$ for low-viscosity regimes ($Oh \lesssim 0.1$) and $\beta_m \sim Re^{1/5}$ for high-viscosity regimes ($Oh > 1$), where We, Re and Oh are the Weber, Reynolds and Ohnesorge numbers, respectively. Both scaling laws show good agreement with the experimental data for their respective validity ranges of Oh. Furthermore, to better model experimental data at vanishing Re, we introduce a semi-empirical scaling law, $\beta_m \sim (A + We/Oh)^{1/6}$, where A is a fitting parameter accounting for finite spreading ($\beta_m \approx 1$) at negligible impact velocities. This semi-empirical law provides an effective description of β_m for a broad experimental range of $10^{-3} \leqslant Oh \leqslant 10^0$ and $10^1 \leqslant We \leqslant 10^3$.

Key words: drops and bubbles, drops

1. Introduction

The impact of liquid droplets on solid surfaces is a common and vital process in both nature and industry, not only displaying fascinating fluid dynamics but also significantly influencing numerous applications (Yarin 2006; Quéré 2013; Josserand & Thoroddsen

2016; Lohse 2022). For instance, raindrop impacts contribute to soil erosion (Soto *et al.* 2014), while the effectiveness of spray cooling is profoundly affected by drop impact dynamics (Breitenbach, Roisman & Tropea 2018). Among the various intriguing impact outcomes, such as rebound, splashing, jetting and atomisation (Rioboo, Tropea & Marengo 2001; Tsai *et al.* 2009, 2010; Thoroddsen, Takehara & Etoh 2012; Burzynski, Roisman & Bansmer 2020; Jha *et al.* 2020; García-Geijo *et al.* 2021; Liu *et al.* 2022; Ma *et al.* 2024), the most common outcome is droplet spreading (Rioboo *et al.* 2001; Lagubeau *et al.* 2012; Lolla *et al.* 2022; Liu *et al.* 2023).

Droplet spreading is typically quantified by the maximum spreading factor ($\beta_m = D_m/D_0$) (Clanet *et al.* 2004; Laan *et al.* 2014; Liu *et al.* 2018; Gordillo, Riboux & Quintero 2019), defined as the ratio of the maximum spreading diameter (D_m) to the initial droplet diameter (D_0). This factor is critical in applications such as printing, coating, and cooling. Due to its importance, various models have been developed to better understand and predict β_m. These models rely on theoretical analyses using energy or momentum conservation (Pasandideh-Fard *et al.* 1996; Clanet *et al.* 2004; Lee *et al.* 2016*b*; Wildeman *et al.* 2016; Yonemoto & Kunugi 2017; Huang & Chen 2018; Gordillo *et al.* 2019; Du *et al.* 2021; Aksoy *et al.* 2022), mass balance (Roisman 2009) and empirical fits to experimental data (Scheller & Bousfield 1995; Bayer & Megaridis 2006; Sen, Vaikuntanathan & Sivakumar 2014; Lee *et al.* 2016*c*; Tang *et al.* 2017; Liang *et al.* 2019; Singh *et al.* 2021), incorporating dimensionless numbers such as the Weber (*We*), Reynolds (*Re*) and Ohnesorge (*Oh*) numbers, defined as

$$We = \frac{\rho D_0 U_0^2}{\sigma}, \quad Re = \frac{\rho D_0 U_0}{\mu} \quad \text{and} \quad Oh = \frac{\mu}{\sqrt{\rho D_0 \sigma}} = \frac{\sqrt{We}}{Re}, \quad (1.1)$$

where U_0 is the impact velocity; ρ, σ and μ are the droplet's density, surface tension and dynamic viscosity, respectively. Here, *We* and *Re* compare inertial forces with capillary and viscous forces, respectively. *Oh* relates viscous forces to inertial-capillary forces (Josserand & Thoroddsen 2016), representing the dimensionless viscous effect (Sanjay & Lohse 2025), and also characterises the ratio of the viscous-capillary time scale ($\tau_\mu \sim \mu D_0/\sigma$) to the inertial-capillary time scale ($\tau_R \sim \sqrt{\rho D_0^3/\sigma}$) (Bartolo, Josserand & Bonn 2005; Lin *et al.* 2018). The high-*Oh* regime typically corresponds to $Oh \gtrsim 1$, where viscous forces dominate over inertial and capillary effects, strongly influencing the spreading dynamics.

Based on the concept of energy conservation, the droplet's initial kinetic and surface energies are converted into final surface energy at β_m and viscous dissipation. Pasandideh-Fard *et al.* (1996) proposed a model for β_m, suggesting that viscous dissipation occurs primarily in the boundary layer (BL) at the droplet–surface interface, with the BL thickness approximated as $\delta = 2D_0/\sqrt{Re}$. When $We > 12$ and $We \gg \sqrt{Re}$, this model simplifies to the scaling law $\beta_m \sim Re^{1/4}$. Our experimental data for ionic liquids with viscosities around 30 mPa s are consistent with this scaling law (Liu *et al.* 2023). However, in the high-viscosity regime, the BL approximation would suggest a physically inconsistent BL thickness, exceeding D_0. To address this, different BL thickness scales have been proposed for low- and high-viscosity droplets (Mao, Kuhn & Tran 1997; Sanjay & Lohse 2025). For high-viscosity liquids, the height of the deformed pancake-shaped droplet at β_m, estimated from the mass balance as $h \sim D_m^3/D_0$, is used as the velocity-gradient depth to approximate the dissipation term. This approach yields the scaling law $\beta_m \sim Re^{1/5}$ (Madejski 1976; Clanet *et al.* 2004), which is consistent with the experimental data for high-viscosity liquids (Clanet *et al.* 2004; Liu *et al.* 2023). Recently, Jørgensen (2024) proposed that the maximum value of the droplet contact

diameter (D_c) on the surface scales with $Re^{1/3}$ at $Re < 1$, based on the energy conservation principles and the assumption that the BL thickness scales with D_c in this regime.

In the capillary regime, where viscous dissipation is low and negligible, the initial kinetic energy is converted into surface energy, leading to $\beta_m \sim We^{1/2}$ (Clanet *et al.* 2004). Alternatively, by balancing impact and capillary forces (Cheng 1977) or applying momentum and volume conservation (Clanet *et al.* 2004), the scaling law $\beta_m \sim We^{1/4}$ is obtained, which agrees with the experimental results for millimetre-sized water drops on flat surfaces (Clanet *et al.* 2004; Tsai *et al.* 2011; Laan *et al.* 2014; Liu, Cai & Tsai 2020; Wang *et al.* 2022b). As a result, Clanet *et al.* (2004) proposed $\beta_m \sim We^{1/4}$ for the capillary regime and $\beta_m \sim Re^{1/5}$ for the viscous regime, with a critical transition point defined as $P^\star = WeRe^{-4/5} = 1$ (Bartolo *et al.* 2005). In response, Wang *et al.* (2022a) proposed a universal expression of $\beta_m Re^{-1/5} = (P^{\star 1/4} + A_2 P^{\star 1/2})/(A_1 + P^{\star 1/4} + A_2 P^{\star 1/2})$, where A_1 and A_2 are fitting parameters. Differently, Eggers *et al.* (2010) suggested a different transition boundary at $P = WeRe^{-2/5}$, where $\beta_m \sim We^{1/2}$ applies in the capillary regime. A universal expression of $(D_m/D_0)Re^{-1/5} = P^{1/2}/(A + P^{1/2})$ (where A is a fitting constant) was then proposed (Laan *et al.* 2014). However, recent experimental (Lee *et al.* 2016a; Liu *et al.* 2023) and numerical (Sanjay & Lohse 2025) data, across various We, Re and Oh values, show that these universal formulas (Laan *et al.* 2014; Wang *et al.* 2022a) effectively describe β_m in low-Oh regimes and at high-impact velocities, indicating the need for further investigation into β_m under a broader range of impact conditions.

In terms of empirical fitting, Scheller & Bousfield (1995) introduced a regression model correlating β_m with $Re^2 Oh$, which fits experimental data well with the expression $\beta_m \sim (Re^2 Oh)^{0.166}$ for droplets with a viscosity range of $2.5 \leqslant \mu \leqslant 25$ mP s. Since $Re^2 Oh$ encompasses kinetic, surface and viscous energies, the formula of $\beta_m = a(Re^2 Oh)^b$, or equivalently $\beta_m = a(We/Oh)^b$, has been frequently used to fit experimental data, where a and b are fitting parameters dependent on liquid properties (Sen *et al.* 2014; Seo *et al.* 2015; Liang *et al.* 2019), surface roughness (Tang *et al.* 2017; Singh *et al.* 2021) and surface wettability (Bayer & Megaridis 2006).

Our previous experiments on viscous ionic liquid droplets impacting flat surfaces revealed distinct fits of β_m scaling: $\beta_m \sim Re^{1/4}$ for low-viscosity droplets and $\beta_m \sim Re^{1/5}$ for high-viscosity droplets (Liu *et al.* 2023). Given the partial good agreement between experimental data and existing universal scaling laws, we hypothesise that β_m behaviour for viscous droplets may vary across different regimes. In this study, we experimentally and theoretically investigate the maximum spreading of viscous droplets on flat surfaces upon impact under a broad range of parameters, including wide liquid viscosities ($1 \leqslant \mu \leqslant 1, 216$ mPa s) and impact velocities ($0.2 \leqslant U_0 \leqslant 4.5$ m s^{-1}).

2. Experimental

To investigate the influence of liquid viscosity on droplet spreading, silicone oil (Sigma–Aldrich) and mixtures of glycerol (Aladdin) and Milli-Q® water at different mass ratios were prepared, with pure water included for comparison. All experiments were conducted at atmospheric pressure and room temperature. The surface tension and dynamic viscosity of the solutions were measured using a surface tensiometer (Shanghai Fangrui, BZY100) and a rotational viscometer (Shanghai Fangrui, NDJ-5s), respectively. Liquid density was calculated from separate measurements of mass and volume. The measured properties are given in table 1.

Droplets were generated using a blunt needle connected to a syringe pump. Each droplet, with an initial diameter D_0, detached from the needle once its gravitational force exceeded

Liquid	Density ($g\,cm^{-3}$)	Dynamic viscosity (mPa s)	Surface tension ($mN\,m^{-1}$)	Ohnesorge number
G-W 0 %	1.00	1.0	72.0	0.002
G-W 30 %	1.08	2.6	53.2	0.006
G-W 45 %	1.12	4.6	54.3	0.011
G-W 60 %	1.16	10.3	57.8	0.023
G-W 70 %	1.18	22.1	59.3	0.050
G-W 80 %	1.19	55.2	60.4	0.123
G-W 82.5 %	1.20	72.9	60.5	0.162
G-W 85 %	1.21	98.7	62.7	0.215
G-W 87.5 %	1.22	132.3	62.7	0.288
G-W 90 %	1.23	193.4	62.5	0.421
G-W 92.5 %	1.24	224.0	62.9	0.484
G-W 95 %	1.24	397.1	62.8	0.858
G-W 100 %	1.25	1216.1	62.6	2.630
Silicon oil	0.97	500.0	21.1	2.738

Table 1. The density (ρ), dynamic viscosity (μ), surface tension (σ) and the corresponding Ohnesorge number (Oh) of the glycerol–water (G-W) mixtures and silicone oil at room temperature. The percentage shown in the table is the weight percentage of the glycerol.

surface tension. The droplet then fell freely and impacted the solid surface with an impact velocity U_0, measured from high-speed camera snapshots using image analysis. The value of U_0 was varied by adjusting the free-fall height and ranged from 0.20 to 4.52 m s^{-1}. The dimensionless parameters explored here include: $2 \leqslant We \leqslant 1$, 194, $0.5 \leqslant Re \leqslant 13$, 476 and $0.002 \leqslant Oh \leqslant 2.738$. A flat glass with an average roughness of 0.5 nm was used as the solid surface. A high-speed camera (Photron SA-X2), operating at 10 000 frames per second, recorded the impact dynamics from the side view, with backlighting provided by an LED light (Phlox LEDW). All data were extracted from high-speed images using a customised ImageJ (Schindelin *et al.* 2012) code. The pixel resolution in our experiments was 19.2 µm pixel^{-1}. The maximum error in the measurement of β_m is approximately 5 %, based on the estimated errors from image binarisation and three repeated measurements. Since the error bars are too small to be visible, they are not included in the figures.

3. Viscous droplets impact on flat surfaces

3.1. *Spreading on a flat surface*

In the range of experimental parameters explored, we observed two types of impact outcomes: spreading, where the droplet spreads (while simultaneously oscillating) upon contact, reaches its maximum spreading diameter of the lamella, D_m (see figure 1), and eventually adheres to the surface; and splashing, where secondary droplets are ejected from the advancing lamella during spreading. For a concise analysis of β_m, data with splashing outcomes were excluded. Figure 1 shows sequential snapshots of glycerol–water droplets spreading on a flat surface at the same U_0. Phenomenologically, while undergoing simultaneous droplet oscillation (Banks *et al.* 2014), low-viscosity droplets spread and flatten into circular disks (figures 1*a* and 1*b*), whereas high-viscosity droplets rapidly form ellipsoids and reach D_m (figure 1*c*). Here, we focus on the analysis of early-time β_m, while simultaneously the drop naturally oscillates upon impact for an extended period (Bechtel, Bogy & Talke 1981; Fukai *et al.* 1993; Banks *et al.* 2014; Das *et al.* 2019; McCarthy, Reid &
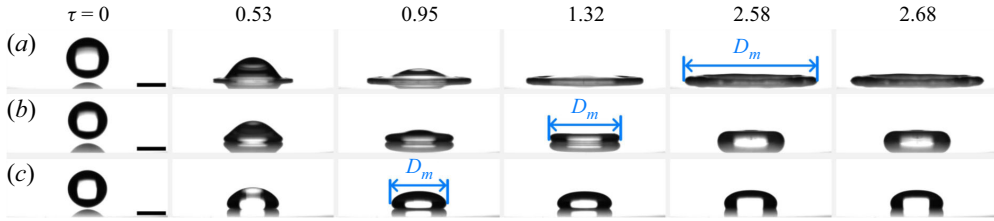
Figure 1. Sequential snapshots of glycerol–water droplets impacting a flat surface at the same impact velocity of $U_0 = 1.52 \, \mathrm{m\,s^{-1}}$ for (a) $Oh = 0.006$, (b) $Oh = 0.215$ and (c) $Oh = 0.858$. The maximum spreading diameter (D_m) occurs at $\tau = 2.58$, $\tau = 1.32$ and $\tau = 0.95$ for (a), (b) and (c), respectively. Here, the dimensionless time $\tau = t/\tau_i$, where t is the time, and $\tau_i = D_0/U_0$ represents the characteristic impact time. The inset scale bars are 2 mm.
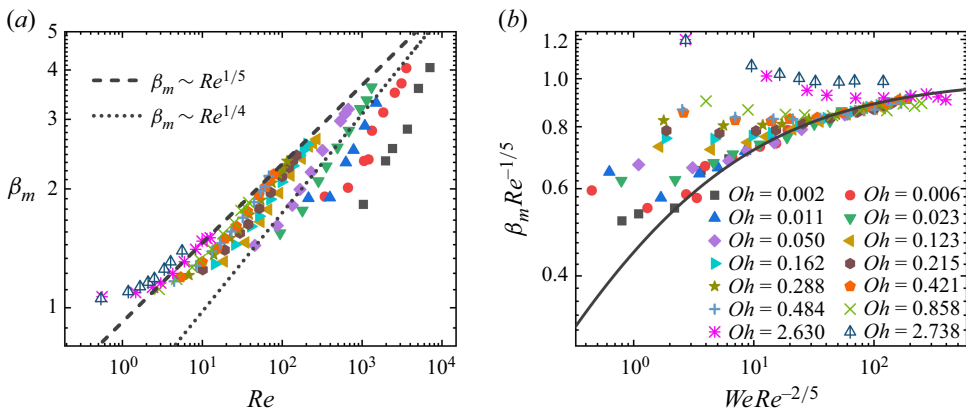

Figure 2. Variations of the experimental maximum spreading factor, β_m, with (a) Reynolds number (Re) and (b) impact parameter $P = WeRe^{-2/5}$ for different glycerol–water droplets. The dashed and dotted lines in (a) represent $\beta_m \sim Re^{1/5}$ and $\beta_m \sim Re^{1/4}$, respectively. The solid line in (b) refers to the expression of $\beta_m Re^{-1/5} = P^{1/2}/(A + P^{1/2})$, with $A = 1.24$ (Laan *et al.* 2014).

Walker 2023). As expected, D_m decreases with increasing liquid viscosity (i.e. *Oh*) at the same U_0 due to enhanced viscous dissipation.

Figure 2 shows our experimental maximum spreading factor ($\beta_m = D_m/D_0$) varying with *Re* and impact number of $P = WeRe^{-2/5}$ (Laan *et al.* 2014). The results reveal good agreement with $\beta_m \sim Re^{1/4}$ in the medium-viscosity regime and $\beta_m \sim Re^{1/5}$ in the high-viscosity regime. However, neither scaling law fully captures β_m across the entire viscosity range examined.

A comparison of our experimental data with the universal expression proposed by Laan *et al.* (2014) shows that the model is consistent with our data in the low-*Oh* and high-U_0 ranges (see figure 2b). Our findings are also consistent with recent numerical investigations of β_m (see figure 1b reported by Sanjay & Lohse (2025)), spanning a broad range of *We* ($1 \leqslant We \leqslant 10^3$) and *Oh* ($10^{-3} \leqslant Oh \leqslant 10^2$). Additional comparisons between our experimental β_m and existing scaling laws from the literature (Cheng 1977; Pasandideh-Fard *et al.* 1996; Clanet *et al.* 2004; Ukiwe & Kwok 2005; Roisman 2009; Wang *et al.* 2022a) are provided in figures S1–S3 of the supplementary material (available at https://doi.org/10.1017/jfm.2025.10550), showing that these models align with the data in specific (partial) parameter ranges.

L. Liu, G. Cai, W. Wang, B. He and P.A. Tsai

3.2. *Modelling of maximum spreading factor (β_m)*

This study focuses on viscous droplets, where viscosity dominates the entire drop impact process. By analysing total energy conservation, β_m can be estimated or predicted by converting the initial total energy of the impacting droplet (comprising its initial kinetic and surface energies) into the final energy of the deformed droplet at β_m (covering viscous dissipation and final surface energy, with negligible liquid velocity or kinetic energy). The viscosity dissipation can arise from bulk liquid dissipation (Clanet *et al.* 2004; Attané *et al.* 2007; Sanjay & Lohse 2025) and moving contact-line dissipation (Attané *et al.* 2007; Snoeijer & Andreotti 2013; Carlson *et al.* 2012*a,b*; Wang, Amberg & Carlson 2017). However, we assume that the latter can be neglected for high-speed and viscous droplets, as discussed in Appendix A.2. In addition, the change in the droplet–surface energy (ΔE_s) compared with the initial kinetic energy (E_k) is assumed to be insignificant for $We > 10$ (see Appendix A.1 for detailed analyses).

In this context, with our simplified energy conservation, the initial kinetic energy (E_k) of the impacting droplet is dissipated by viscosity at β_m, where

$$E_k = mU_0^2/2 \sim \rho D_0^3 U_0^2, \tag{3.1}$$

where m is the droplet mass. The energy dissipation due to viscosity (E_μ) upon reaching β_m can be approximated as (Chandra & Avedisian 1991; Pasandideh-Fard *et al.* 1996):

$$E_\mu = \int_0^{t_m} \int_V \phi \, dV \, dt, \tag{3.2}$$

where V is the viscous fluid volume where significant viscous dissipation occurs; the duration to reach β_m is approximated as $t_m \sim R_m/U_o$, which shows good consistency with our experimental observations (see detailed discussion in Appendix B); here, $R_m = D_m/2$ is the maximum spreading radius; ϕ is the dissipation function that represents the rate of viscous dissipation per unit volume, expressed as (Kundu & Cohen 2002)

$$\phi = \frac{\mu}{2} \left(\frac{\partial v_r}{\partial z} + \frac{\partial v_z}{\partial r} \right)^2, \tag{3.3}$$

where $\partial v_r/\partial z$ and $\partial v_z/\partial r$ represent the gradients of the radial and vertical velocity components, v_r and v_z, respectively. Numerical results by Lee *et al.* (2016*a*); Sanjay *et al.* (2025) have shown that the velocity field within a spreading droplet varies both spatially and temporally, and so does the viscous dissipation function ϕ. To simplify the analysis, in this study $\partial v_z/\partial r = 0$ is assumed (Roisman 2009), and (3.3) is reduced to $\phi \approx \mu(\partial v_r/\partial z)^2$.

For scaling purposes, the radial velocity v_r is approximated by the speed of the spreading lamella, denoted $V_s = dD_s/dt$, where D_s is the spreading lamella diameter (see figure 3*a* schematic). Our experimental data show that the evolution of D_s closely follows that of the contact diameter, D_c; thus, we approximate $V_s \approx dD_c/dt$ (see supplementary material for detailed discussion).

Figure 3 shows the evolution of drop spreading dynamics for various *Oh*. Initially, droplets spread rapidly within the characteristic impact (or inertial) time ($\tau_i = D_0/U_0$) and then saturate to the maximum value. The contact diameter can be expressed as $D_c(t) = \sqrt{c_d U_0 R_0 t}$ (where R_0 is the initial radius of the droplet) based on geometrical considerations (Mongruel *et al.* 2009) or Wagner's theory (Riboux & Gordillo 2014), where c_d is a prefactor. Our empirical fits of $D_c(t)$ agree with this scaling law for $t/\tau_i < 1$ (see figure 3). Differentiating $D_c(t)$ with respect to time provides the approximation of $V_s \approx dD_c/dt \sim \sqrt{U_0 D_0/t}$, which, when evaluated at $t \sim \tau_i$, leads to the approximation of $V_s \sim U_0$.
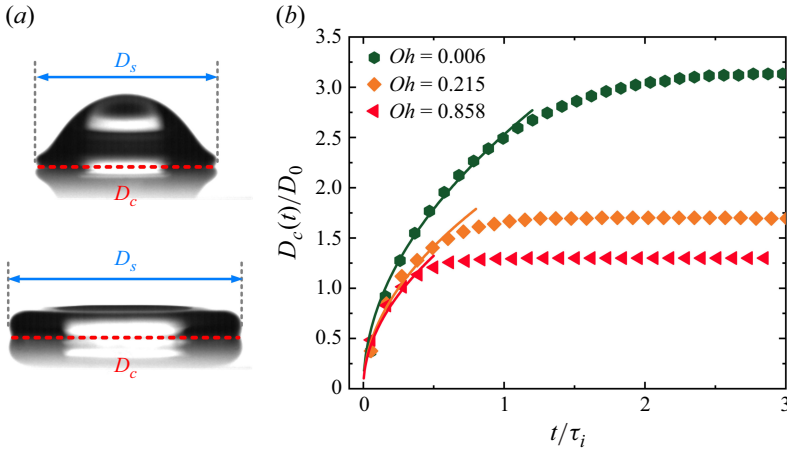
Figure 3. (*a*) Schematic of the spreading diameter of the advancing lamella (D_s) and the contact-line diameter (D_c). (*b*) Variation of normalised contact diameter, $D_c(t)/D_0$, with a dimensionless impact time, t/τ_i, at $U_0 = 1.52$ m s^{-1} for various Ohnesorge (*Oh*) numbers; here, $\tau_i = D_0/U_0$. The measurement error of D_c is $\approx 7.7\,\%$ (see supplementary material for more details on the measurement error). The solid lines represent the empirical fits of $D_c(t)/D_0 \sim \sqrt{t/\tau_i}$ or $D_c(t) \sim \sqrt{U_0 D_0 t}$, with varying prefactors.

Before detailedly analysing E_μ (3.2), we briefly review the drop impact process based on recent studies of impact force dynamics (Gordillo, Sun & Cheng 2018; Cheng, Sun & Gordillo 2021; Zhang *et al.* 2022; Sanjay *et al.* 2025). When a viscous droplet impacts a wetted solid surface, such as glass in this study, the impact force rapidly increases, peaking at time τ_ρ. The force then decays over a longer time scale as the droplet spreads radially, eventually reaching D_m as the impact force diminishes to zero. The impact force decelerates the droplet's vertical motion, redirecting vertical momentum into radial flow and, hence, playing a critical role in viscous dissipation. The drop impact process can hence be characterised into two phases: the impact phase and the spreading phase, separated by the time boundary τ_ρ, and the duration of the impact phase is typically shorter compared with the spreading period (Sanjay & Lohse 2025). Furthermore, numerical studies have shown that viscous dissipation during the impact phase can account for a proportion of the total energy dissipation (Wildeman *et al.* 2016). More recently, a unifying theoretical model has been developed based on numerical data, which analyses the temporal evolution of viscous dissipation contributions during both the impact and spreading phases (Sanjay & Lohse 2025). These dissipation contributions are modelled to be localised within the BL or distributed throughout the drop bulk, depending on the governing parameter regimes of *We* and *Oh* (Sanjay & Lohse 2025).

Our current experimental results, focusing on side-view measurements of spreading dynamics, do not provide time-resolved internal velocity fields or impact force measurements. We are currently unable to directly track the evolution or spatial distribution of viscous dissipation within the droplet. Future experimental studies using techniques such as particle image velocimetry (PIV) or other flow diagnostic tools would be valuable for quantitatively characterising the velocity field and identifying the regions and timing of dissipation. Given this limitation, we adopt a simplified framework that considers two limiting regimes.

In our theoretical framework, we analyse two limiting cases: low-viscosity (low-*Oh*) and high-viscosity (high-*Oh*) regimes. In the low-viscosity regime, the BL remains thin, scaling as $\delta \sim \sqrt{\nu t}$, where $\nu = \mu/\rho$ is the drop's kinematic viscosity (Schlichting &

Gersten 2016), and viscous dissipation is assumed to occur within a thin BL adjacent to the liquid–solid interface, where the BL thickness is smaller than the droplet's spreading height. In particular, we assume that the length scale of the BL remains the same for both the impact and spreading phases in this regime. In contrast, in the high-viscosity regime, BL thickness increases, and viscous dissipation is expected to occur throughout the bulk upon impact until reaching β_m.

3.2.1. *High-viscosity (high-Oh) regime*

In the high-viscosity regime, the viscous dissipation is assumed to occur across the droplet's spreading height during both phases, as the experimental observations showed the viscous droplets quickly deform into an ellipsoid shape, reaching D_m. The corresponding spreading height, h_m, satisfies mass conservation, $D_m^2 h_m \sim D_0^3$, assuming the droplet adopts a cylindrical shape during spreading. The viscous dissipation is then approximated as $E_\mu \approx (\mu/2)(V_s/h_m)^2 V t_m \sim \mu(U_0/h_m)D_m^3$ using (3.2) and (3.3), where $V_s \sim U_0$, $V \approx \pi D_m^2 h_m/4$ and $t_m \sim R_m/U_0$.

Energy conservation, by balancing the initial kinetic energy (E_k) (3.1) with this viscous dissipation, gives rise to $\beta_m \sim Re^{1/5}$ as previously derived by Clanet *et al.* (2004). As shown in figures 2(*a*) and figure 8 in Appendix D, the prediction $\beta_m \sim Re^{1/5}$ agrees with experimental trends for $Oh > 1$ and $Re > 2$, indicating that the high-viscous regime is applicable for $Oh > 1$ empirically. However, as listed in table 1, only 100 % glycerol and silicon oil have $Oh > 1$, suggesting that additional studies with $Oh > 3$ are encouraged to further validate this power law.

3.2.2. *Low-viscosity (low-Oh) regime*

For the low-viscosity regime, viscous dissipation is assumed to be localised within a thin BL during the entire t_m. Within this BL, a velocity gradient $\partial v_r/\partial z$ exists, and the relevant dissipation function ϕ in (3.3) for this regime is approximated as

$$\phi \approx \mu \left(\frac{\partial v_r}{\partial z} \right)^2 \sim \mu \left(\frac{U_0}{\delta} \right)^2, \tag{3.4}$$

where δ represents the BL thickness.

In the literature, various expressions for δ have been considered to estimate viscous dissipation analytically. Pasandideh-Fard *et al.* (1996) proposed $\delta = 2D_0/\sqrt{Re}$, based on stagnation-point flow. Alternatively, Eggers *et al.* (2010) suggested $\delta = \sqrt{\nu t}$, where $\nu = \mu/\rho$ is the kinematic viscosity. Numerical studies by Lee *et al.* (2016a) and Philippi, Lagrée & Antkowiak (2016) further indicated that δ varies both spatially and temporally. For simplicity, Wildeman *et al.* (2016) approximated $\delta = \sqrt{\nu t_{sp}}$, where t_{sp} represents the time to reach β_m and is estimated from their numerical data.

Both experimental studies (Banks *et al.* 2014; McCarthy *et al.* 2023) and numerical simulations (Bechtel *et al.* 1981; Fukai *et al.* 1993; Das *et al.* 2019) show that an inviscid droplet (e.g. water) oscillates upon impacting a solid surface, with the oscillation frequency (ω) proportional to the natural free oscillation frequency (ω_0), i.e. $\omega \approx \omega_0 \sim \sqrt{\sigma/(\rho D_0^3)}$, with surface tension σ acting as the restoring force (Fukai *et al.* 1993; Marmanis & Thoroddsen 1996). For viscous droplets, this frequency is damped to $\omega_\mu \sim \omega_0\sqrt{1 - 25Oh^2/4}$ (Prosperetti 1980; Tonini & Cossali 2024) due to viscous dissipation. However, in the low-viscosity (low-Oh) regime, the influence of viscous dissipation on ω is negligible, i.e. $\omega \approx \omega_0$, consistent with similar experimental findings for $Oh \leqslant 0.174$ (Banks *et al.* 2014).
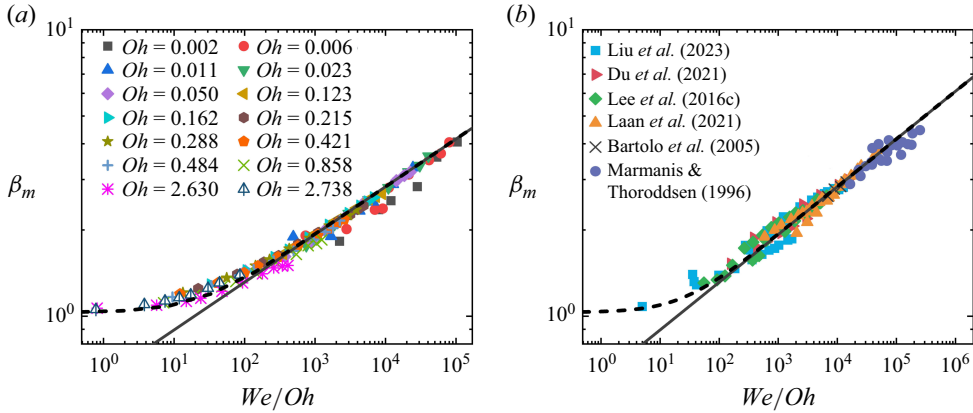
Figure 4. (*a*) Variations of the maximum spreading factor, β_m, with We/Oh. (*b*) Experimental data of β_m extracted from the literature for viscous droplets. The solid and dashed lines represent $\beta_m = 0.61(We/Oh)^{1/6}$ (3.6) and $\beta_m = 0.61(23.3 + We/Oh)^{1/6}$ (3.7), respectively, where the prefactor 0.61 is obtained empirically.

As a major assumption, we assume that an oscillatory BL forms during droplet impact, as our (see figure 7 later) and others (Banks *et al.* 2014; McCarthy *et al.* 2023) experiments show that droplet oscillations are initiated upon impact. This behaviour may be analogous to the classical second Stokes BL problem (Schlichting & Gersten 2016), where a BL develops in response to an oscillating wall. Similarly, in an oscillating droplet, an oscillatory BL may form near the substrate (Bechtel *et al.* 1981; Kim & Chun 2001). Based on this analogy, we approximate the BL thickness using the classical Stokes formulation, $\delta \sim \sqrt{2\mu/(\rho n)}$ (Bechtel *et al.* 1981; Batchelor 2000; Schlichting & Gersten 2016), where $n = 2\pi\omega = 2\pi/t_{osc}$ is the angular frequency, resulting in $\delta \sim \sqrt{\nu t_{osc}}$. By substituting $t_{osc} \sim 1/\omega_0$ for low-viscosity droplets, we obtained an expression for the BL thickness:

$$\delta \sim \sqrt{\nu t} \sim D_0 Oh^{1/2}. \tag{3.5}$$

With energy conservation ($E_k \sim E_\mu$) at β_m, using (3.1), (3.2), (3.4), (3.5), t_m-approximation of R_m/U_0, and the viscous fluid volume of $V = \pi D_m^2 \delta/4$, we derive

$$\beta_m = \frac{D_m}{D_0} \sim (Re^2 Oh)^{1/6} = (We/Oh)^{1/6}, \tag{3.6}$$

for the β_m scaling in the low-viscosity (low-Oh) regime. This theoretical expression of (3.6) interestingly matches the empirical regression model fitted by Scheller & Bousfield (1995) for glycerol–water mixtures with a viscosity range of $2.5 \leqslant \mu \leqslant 25$ mPa s.

Figure 4(*a*) shows experimental β_m varying with We/Oh, demonstrating good agreement with the scaling law (3.6) for $Oh \lesssim 0.1$ under the We/Oh range explored, as represented by the solid line in figure 4(*a*). However, since surface energy is not considered in (3.6), β_m for Milli-Q® water ($Oh = 0.002$) and the 30 % glycerol–water mixture ($Oh = 0.006$) with the low-viscosity (box and circle in figure 4*a*) deviates from (3.6) at lower-U_0 values. For these cases, the energy conservation equation should account for surface energy change: $E_k - \Delta E_s = E_\mu$, where ΔE_s is the surface energy difference between the initial state and at β_m and can be approximated as $\Delta E_s \sim \sigma(D_m^2 - D_0^2)$ (see Appendix A.1 for details). At the low-Oh and low-U_0 ranges, ΔE_s and E_k become comparable, and excluding ΔE_s from the model overestimates β_m.

Moreover, our experimental data show that the scaling law $\beta_m \sim (We/Oh)^{1/6}$, derived under the assumption of viscous dissipation occurring within a thin BL, remains applicable

for the moderate-*Oh* ($0.1 < Oh < 1$) and high-*We* ($We > 155$) regime. We interpret this as follows: although viscosity is non-negligible, the maximum spreading time t_m becomes shorter with increasing U_0, as shown later in figure 6. Consequently, the dissipation region ($\delta \sim \sqrt{\nu t}$) may not have sufficient time to grow beyond the boundary layer thickness before maximum spreading is reached. This suggests that, even at the moderate-*Oh* and high-*We* range, viscous dissipation remains confined to the BL, supporting the applicability of the boundary-layer-based scaling in this regime.

3.2.3. *Semi-empirical scaling model*

Returning to (3.6), this theoretical scaling law predicts $\beta_m = 0$ as $We/Oh = 0$. However, in practice, the maximum spreading diameter (D_m) tends to be D_0 as the droplet deposits gently onto a surface with negligible velocity ($U_0 \approx 0$). Physically, β_m should converge to a finite value (i.e. 1) as $We/Oh \to 0$. To incorporate this finite spreading as $U_0 \to 0$, (3.6) is mathematically modified to be

$$\beta_m \sim (A + We/Oh)^{1/6}, \tag{3.7}$$

where A is a constant. By applying $\lim_{We/Oh \to 0} \beta_m = 1$, we obtain $A = 23.3$. Remarkably, we found that the semi-empirical model in (3.7) consistently aligns with our experimental data for the wide-viscosity range explored, as revealed by the dashed line in figure 4(*a*). We further validate our models with the existing experimental data from the literature, as presented in figure 4(*b*). The good agreement between our semi-empirical model (3.7) and various data under wide-ranging parameters ($10^{-3} \leqslant Oh \leqslant 10^0$ and $10^1 \leqslant We \leqslant 10^3$) highlights the good application of our model for viscous droplet spreading on a flat solid surface.

We further compare our experimental data and semi-empirical model with the universal prediction proposed recently by Sanjay & Lohse (2025), as shown in figure 5. The comparative results show that the universal prediction by Sanjay & Lohse (2025) agrees well with our experimental data across most of the parameter space (figures 5*a–e*). Our semi-empirical model (3.7) also yields consistent results with those of Sanjay & Lohse (2025) for most range of *Oh* from 0.01 to 10 (see figure 5*a–f*), except in two regimes: (i) at low *Oh* ($= 0.01$), relatively low *We* ($1 - 20$) (figure 5*a*) and (ii) at high *Oh* ($= 10$), relatively high *We* (>100) (figure 5*f*).

In the low-*Oh* and relatively low-*We* regime (see figure 5*a*), the droplet's surface energy difference (ΔE_s) can play a non-negligible role. While the model of Sanjay & Lohse (2025) explicitly incorporates ΔE_s in the energy balance analysis, our semi-empirical formulation does not. Consequently, our model (dashed line) tends to overestimate the maximum spreading factor β_m in this regime.

In the high-*Oh* regime (see figure 5*f*), at $Oh = 10$ the prediction by Sanjay & Lohse (2025) exhibits a flattening trend, with $\beta_m \approx 1$ indicating that most of the initial kinetic energy is dissipated primarily during the impact phase (Sanjay & Lohse 2025). Under such conditions, increases in *We* no longer contribute significantly to spreading. Our experimental data are currently limited in these two regimes, and future experimental studies are needed to investigate β_m variation in the low-*Oh* and low-*We* regime and to confirm the limiting spreading as $D_m \approx D_0$ at high *Oh* ($\gtrsim 10$).

4. Conclusions

The maximum spreading factor of viscous droplets impacting solid surfaces has been systematically investigated across a wide range of *We*, *Re* and *Oh*. For the broad viscosity range of $\mu = 1 - 1216$ mPa s explored, the spreading dynamics is predominantly governed
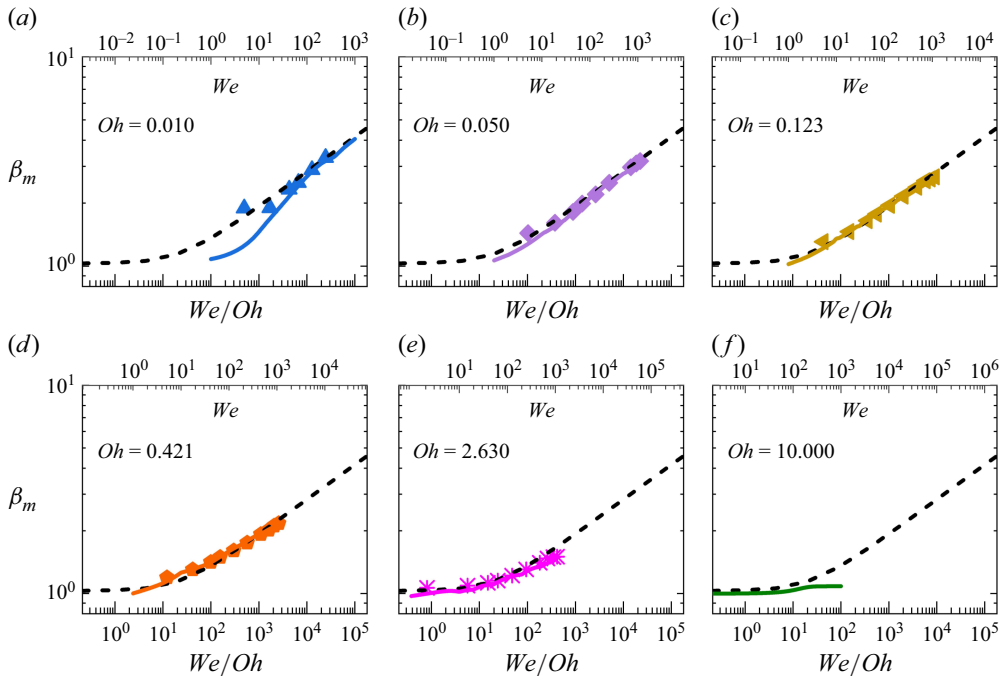
Figure 5. Comparison among our experimental data (symbols), our semi-empirical model (dashed line), and the universal prediction (solid lines) proposed by Sanjay & Lohse (2025), across various Oh and We. The universal prediction is obtained at a specific Oh while varying We from 1 to 1000. Here, the experimental data points are the same as in figure 4(*a*). The dashed line represents our semi-empirical model $\beta_m = 0.61(23.3 + We/Oh)^{1/6}$ (3.7).

by liquid viscosity. We theoretically consider two limiting regimes: viscous dissipation occurring within a BL adjacent to the liquid–solid interface for low-viscosity droplets and throughout the entire bulk of droplet spreading height for high-viscosity droplets. By applying energy conservation principles, where the initial kinetic energy is fully dissipated due to liquid viscosity, scaling laws for β_m are derived: $\beta_m \sim (We/Oh)^{1/6}$ for the low-viscosity regime and $\beta_m \sim Re^{1/5}$ for the high-viscosity regime. Our experimental data indicate that the former scaling law is valid for $Oh \lesssim 0.1$ (low-viscosity range), whereas the latter is applicable for $Oh > 1$ (high-viscosity range) and $Re > 2$. These validity ranges of Oh delineating the low- and high-viscosity regimes are determined empirically. Experimental data further show that $\beta_m \sim (We/Oh)^{1/6}$ remains applicable at high impact velocities ($We/Oh > 155$) in the intermediate-viscosity range ($0.1 < Oh < 1$). To account for finite spreading as $U_0 \to 0$, a prefactor was introduced, yielding a universal scaling law: $\beta_m \sim (A + We/Oh)^{1/6}$, with $A = 23.3$, determined from the fitting the experimental data. This modification effectively models β_m across the broad range of Oh ($0.002 \leqslant Oh \leqslant 2.738$) explored in this study.

Supplementary material. Supplementary material is available at https://doi.org/10.1017/jfm.2025.10550.

Declaration of interests. The authors report no conflict of interest.

Appendix A. Analysis of the energy budget upon reaching for viscous droplets

Before impact, the total energy of the droplet comprises the initial surface energy (E_s^i) and kinetic energy (E_k) (3.1). During the drop impact process, the viscous dissipation arises due to liquid viscosity and the moving contact line, denoted as E_μ and E_{cl}, respectively. Upon reaching β_m, the kinetic energy (of the central mass) becomes zero as the spreading velocity vanishes. Comparing the initial impacting and the final deformed state of the droplet, energy conservation can be expressed as

$$E_k + E_s^i = E_s^f + E_\mu + E_{cl}, \tag{A1}$$

where E_s^f is the surface energy at β_m, E_μ and E_{cl} are the viscous dissipation due to the liquid viscosity and the moving contact line, respectively. This equation can be reformulated as

$$E_k = \Delta E_s + E_\mu + E_{cl}, \tag{A2}$$

where $\Delta E_s = E_s^f - E_s^i$ is the change in surface energy.

A.1. *Influence of surface energy change on the energy budget*

The initial surface energy (E_s^i) of a spherical droplet is given by (Pasandideh-Fard *et al.* 1996)

$$E_s^i = 4\pi\sigma R_0^2 \sim \sigma D_0^2. \tag{A3}$$

The surface energy at β_m can be approximated as (Ukiwe & Kwok 2005)

$$E_s^f \approx \pi\sigma D_m h_m + \pi\sigma D_m^2(1 - \cos\theta_Y)/4 \sim \sigma D_m^2, \tag{A4}$$

where h_m is the (minimum) droplet height at β_m, and θ_Y is the Young contact angle. The surface energy difference (ΔE_s) can be approximated as

$$\Delta E_s = E_s^f - E_s^i \sim \sigma\left(D_m^2 - D_0^2\right). \tag{A5}$$

To evaluate the contribution of surface energy difference to the energy budget, we compare ΔE_s with E_k, expressed as

$$\frac{\Delta E_s}{E_k} \sim \frac{\sigma\left(D_m^2 - D_0^2\right)}{\rho D_0^3 U_0^2} = \frac{1}{We}\left(\beta_m^2 - 1\right). \tag{A6}$$

As shown in (A6), the change in surface energy ΔE_s is smaller than the kinetic energy (E_k) at the high-*We* range. Given that β_m decreases with liquid viscosity (see figure S1 in the supplementary material), we hence assume that the ratio of ΔE_s to E_k is negligible for $We > 10$ under our conditions, and exclude surface energy contributions from the energy balance in our simplified theoretical analyses.

A.2. *Viscous dissipation induced by the moving contact line*

The energy dissipation rate at the moving contact line for the drop impact process (Attané *et al.* 2007; Wang *et al.* 2017) ($\dot{E}_{cl}$) can be estimated as

$$\dot{E}_{cl} \sim \int_0^{R_{cl}} \mu_f U_{cl}^2 \mathrm{d}R_{cl}, \tag{A7}$$

where μ_f is the contact-line friction parameter, typically extracted by fitting numerical data to experimental results of drop spreading for each combination of liquid, gas and solid (Wang *et al.* 2017), U_{cl} is the contact-line velocity during drop impact, and R_{cl} is the contact-line radius and can be modelled as $R_{cl} = D_c/2 \sim \sqrt{U_0 D_0 t}$ (see figure 3).

Wang *et al.* (2017) observed that μ_f is relatively insensitive to the impact velocity and has similar magnitudes in both inertial drop impact ($U_0 > 0$) and wetting-driven ($U_0 \approx 0$) cases for a given liquid–solid–air system. Their observations are for water and glycerol–water mixture ($\mu = 10$ mPa s) drops impacting wetting/partial-wetting surfaces (with a static contact angle range of $52° \leqslant \theta_e \leqslant 94°$), under $0.28 \leqslant U_0 \leqslant 1.86$ m s^{-1}. In our case, lacking the empirical values of μ_f for our liquid–surface combination, we approximated its value using results from wetting-driven, dynamic spreading by Yue & Feng (2011); Carlson *et al.* (2012b) as a first-order estimate.

From the dynamic wetting model (Yue & Feng 2011; Carlson *et al.* 2012b), the contact-line velocity ($\overline{u}_{cl}$) for the purely wetting-driven case can be approximated as

$$\overline{u}_{cl} \sim \frac{\sigma}{\mu_f} \frac{\cos\theta_e - \cos\theta}{\sin\theta}, \tag{A8}$$

where θ_e and θ are the equilibrium and dynamic contact angles, respectively. Rearranging, we estimate $\mu_f \sim \sigma/\overline{u}_{cl}$. Using this form and geometric approximation for the spreading of contact-line diameter (Mongruel *et al.* 2009; Riboux & Gordillo 2014), we can approximate $R_{cl}(t) \sim \sqrt{U_0 D_0 t}$ and $U_{cl} = \mathrm{d}R_{cl}/\mathrm{d}t \sim \sqrt{U_0 D_0/t}$. Substituting into the integral form (A7), with scaling approximation we estimate the total contact line (CL) dissipation until t_m:

$$E_{cl} = \int_0^{t_m} \dot{E}_{cl}(t)\mathrm{d}t \sim \int_0^{t_m} \mu_f U_{cl}^2 R_{cl}\mathrm{d}t \sim \frac{\sigma U_0 D_0^{3/2} R_m^{1/2}}{\overline{u}_{cl}}, \tag{A9}$$

where $t_m \sim R_m/U_0$ (see the discussion in Appendix B), and R_m is the maximum spreading radius.

We qualitatively analysed the portion of kinetic energy dissipated by the moving contact line, by comparing the contact-line dissipation (E_{cl}) with the initial kinetic energy ($E_k \sim \rho D_0^3 U_0^2$) of the impacting droplet:

$$\frac{E_{cl}}{E_k} \sim \frac{\sigma R_m^{1/2}}{\overline{u}_{cl} \rho U_0 D_0^{3/2}}. \tag{A10}$$

Due to the lack of a well-characterised friction coefficient (μ_f) under our experimental conditions, it is challenging to accurately estimate the energy contribution from contact-line dissipation (E_{cl}). Our qualitative analysis indicates that the ratio E_{cl}/E_k decreases with increasing U_0 (or *We*), as shown by (A10). At fixed *We*, this ratio also decreases with increasing *Oh*, owing to the experimentally observed decrease in R_m with *Oh* (see figure S1(a) in the supplementary material). The estimation of the ratio E_{cl}/E_k is based on a scaling argument and thus provides a qualitative rather than quantitative measure. Accordingly, in line with commonly adopted assumptions in the literature (Clanet *et al.* 2004; Attané *et al.* 2007; Laan *et al.* 2014; Sanjay & Lohse 2025), here we treat contact-line dissipation as a minor contributor to the total energy loss in our regime of high-*We* and high-*Oh*. Further investigation into the quantitative role of contact-line dissipation (E_{cl}), particularly under varied surface or fluid conditions, may help clarify its potentially regime-dependent contribution.
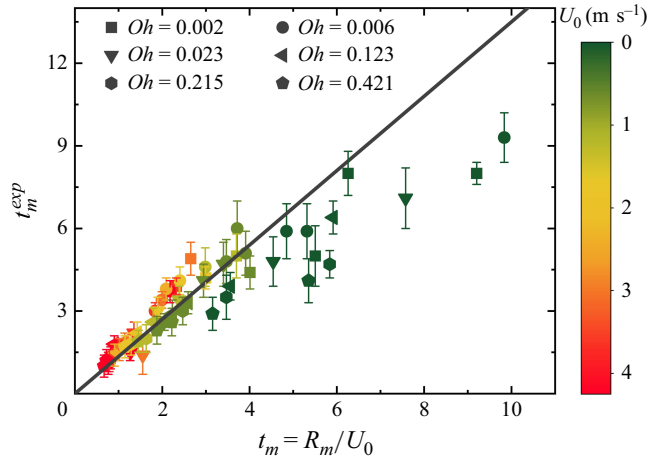
Figure 6. Comparison of the experimental maximum spreading time (t_m^{exp}) and the corresponding theoretical estimation ($t_m = R_m/U_0$) at various Oh and U_0. Here, t_m^{exp} is the time duration obtained directly from the high-speed frames upon reaching the maximum spreading diameter; R_m and U_0 are obtained from the experimental data. The solid line corresponds to $y \sim x$.

In summary, the energy budget (A2) upon reaching β_m for our viscous droplets at $We > 10$ may be approximated as (A11), due to relatively small contributions from ΔE_s and E_{cl} compared with E_k:

$$E_k \approx E_\mu. \tag{A11}$$

Appendix B. The maximum spreading time (t_m)

Our high-speed recordings reveal that the time scale t_m varies with viscosity μ, even when D_0 and U_0 are held constant, as illustrated in figure 1. Theoretically, t_m can be approximated as $t_m \approx R_m/V_s$, where $R_m = D_m/2$ is the maximum spreading radius, and $V_s \sim U_0$ represents the characteristic radial velocity of the spreading lamella (as discussed in the main text). This leads to the scaling $t_m \sim R_m/U_0$, which is consistent with the empirical relation $t_m = bD_m/U_0$ proposed by Lee *et al.* (2016*b*), where b is a fitting coefficient. This expression of t_m also aligns with the use of $t_m \sim D_m/U_0$ by Clanet *et al.* (2004) in their derivation of $\beta_m \sim Re^{1/5}$.

To evaluate the validity of this scaling, we compare our experimentally measured maximum spreading time t_m^{exp}, extracted from high-speed image recordings, with the theoretical estimate $t_m = R_m/U_0$, as shown in figure 6. The data generally follow the expected linear trend, indicating that this scaling serves as a reasonable approximation for the time required to reach β_m across a wide range of conditions. However, an interesting deviation occurs at low U_0, which shows $t_m^{exp}/\tau_i > 1$, and the contact-line velocity U_{cl} – and thus the lamella spreading speed V_s – plateau below U_0 (see figure 3). As a result, the assumption $V_s \sim U_0$ leads to an underestimation of the actual spreading time in this regime, causing those data points to fall below the linear trend. Despite this deviation, the estimate $t_m \sim R_m/U_0$ remains a useful and sufficiently accurate approximation for the maximum spreading time for most data in figure 6, and is therefore adopted in this study.

Appendix C. Droplet oscillation upon impact

Figure 7 shows the typical time evolution of spreading lamella diameter ($D_s(t)$) and spreading central height ($h(t)$). The experimental results suggest that the oscillation is
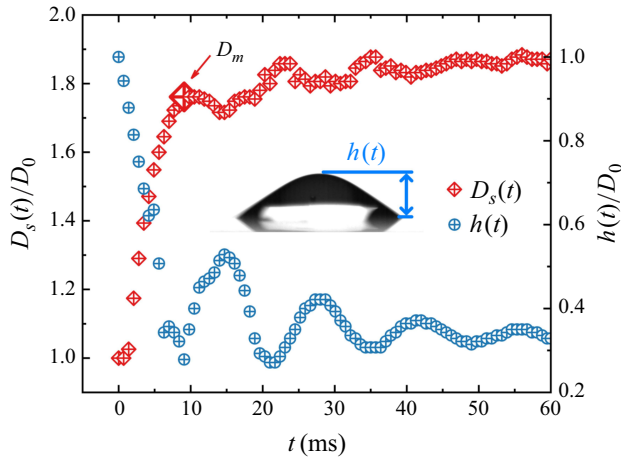
Figure 7. Variation of normalised spreading diameter ($D_s(t)/D_0$) and normalised spreading central height ($h(t)/D_0$) with impact time (t), at an impact velocity of $U_0 = 0.28$ m s^{-1} and $Oh = 0.006$. The inset is a schematic of the spreading height.
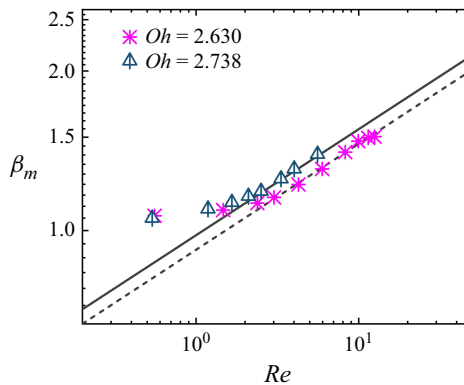

Figure 8. Variations of the maximum spreading factor, β_m, with Re on the flat surface for $Oh > 1$. The solid and dashed lines represent $\beta_m = 0.98Re^{1/5}$ and $\beta_m = 0.92Re^{1/5}$, receptively.

initiated immediately upon contact and persists for up to 60 ms, or possibly longer. The maximum spreading diameter (D_m) is reached at 9.3 ms. As the droplet oscillates, the oscillation amplitude gradually decreases over time due to viscous dissipation.

Because direct measurements of the BL development and thickness remain experimentally challenging, a definitive characterisation of BL structure is currently unavailable. However, based on the observed oscillatory behaviour in both our experiments and numerical simulations, we infer that droplet oscillations are initiated at the moment of impact. Accordingly, as a major assumption, we adopt the Stokes oscillatory BL thickness as an estimate for the characteristic viscous length scale during this stage. More detailed measurements of the velocity field – such as those obtained via PIV – and high-resolution numerical simulations could provide further insight into the development and evolution of the BL in the future, while such efforts are beyond the scope of the present study.

Appendix D. Experimental data in high-viscosity regime ($Oh > 1$)

Figure 8 presents the variation of β_m with Re on a flat glass surface for $Oh > 1$. The results suggest that the theoretical model of $\beta_m \sim Re^{1/5}$ aligns with the experimental β_m for $Oh > 1$ and $Re > 2$. However, the energy conservation becomes complex as $Re < 2$ (the low-U_0 range). In this regime, two factors contribute to the deviation from this theoretical model. First, the work done by the uncompensated Young's force (Carlson *et al.* 2012*a*) becomes comparable to the initial kinetic energy. Second, dissipation at the moving contact line also plays a significant role and should be considered. As a result, the simple balance between the initial kinetic energy and liquid bulk dissipation (A11) cannot fully capture the β_m behaviour in the very low-U_0 range, causing $\beta_m \sim Re^{1/5}$ to deviate from the experimental trend when $Re < 2$.

REFERENCES

AKSOY, Y.T., ENEREN, P., KOOS, E. & VETRANO, M.R. 2022 Spreading of a droplet impacting on a smooth flat surface: how liquid viscosity influences the maximum spreading time and spreading ratio. *Phys. Fluids* **34** (4), 042106.

ATTANÉ, P., GIRARD, F. & MORIN, V. 2007 An energy balance approach of the dynamics of drop impact on a solid surface. *Phys. Fluids* **19** (1), 012101.

BANKS, D., AJAWARA, C., SANCHEZ, R., SURTI, H. & AGUILAR, G. 2014 Effects of liquid and surface characteristics on oscillation behavior of droplets upon impact. *Atomiz. Sprays* **24** (10), 895–913.

BARTOLO, D., JOSSERAND, C. & BONN, D. 2005 Retraction dynamics of aqueous drops upon impact on non-wetting surfaces. *J. Fluid Mech.* **545**, 329–338.

BATCHELOR, G.K. 2000 *An Introduction to Fluid Dynamics*. Cambridge University Press.

BAYER, I.S. & MEGARIDIS, C.M. 2006 Contact angle dynamics in droplets impacting on flat surfaces with different wetting characteristics. *J. Fluid Mech.* **558**, 415–449.

BECHTEL, S.E., BOGY, D.B. & TALKE, F.E. 1981 Impact of a liquid drop against a flat surface. *IBM J. Res. Dev.* **25** (6), 963–971.

BREITENBACH, J., ROISMAN, I.V. & TROPEA, C. 2018 From drop impact physics to spray cooling models: a critical review. *Exp. Fluids* **59**, 1–21.

BURZYNSKI, D.A., ROISMAN, I.V. & BANSMER, S.E. 2020 On the splashing of high-speed drops impacting a dry surface. *J. Fluid Mech..* **892**, A2.

CARLSON, A., BELLANI, G. & AMBERG, G. 2012*a* Contact line dissipation in short-time dynamic wetting. *Europhys. Lett.* **97** (4), 44004.

CARLSON, A., BELLANI, G. & AMBERG, G. 2012*b* Universality in dynamic wetting dominated *b*y contact-line friction. *Phys. Rev. E* **85** (4), 045302.

CHANDRA, S. & AVEDISIAN, C.T. 1991 On the collision of a droplet with a solid surface. *Proc. R. Soc. Lond. A: Math. Phys. Engng Sci.* **432**, 13–41, 1884.

CHENG, L. 1977 Dynamic spreading of drops impacting onto a solid surface. *Ind. Engng Chem. Process Des. Dev.* **16** (2), 192–197.

CHENG, X., SUN, T.-P. & GORDILLO, L. 2021 Drop impact dynamics: impact force and stress distributions. *Annu. Rev. Fluid Mech.* **54**, 57–81.

CLANET, C., BÉGUIN, C., RICHARD, D. & QUÉRÉ, D. 2004 Maximal deformation of an impacting drop. *J. Fluid Mech.* **517**, 199–208.

DAS, S., MOHAMMED, M.I., GIBSON, I., WEERASIRI, L., MCDONNELL, A., XIANG, J. & YEO, L. 2019 Oscillation characteristics of low Weber number impinging micro-droplets. *Theor. Comput. Fluid Dyn.* **33**, 197–213.

DU, J., WANG, X., LI, Y., MIN, Q. & WU, X. 2021 Analytical consideration for the maximum spreading factor of liquid droplet impact on a smooth solid surface. *Langmuir* **37** (24), 7582–7590.

EGGERS J., FONTELOS M.A., JOSSERAND C. & ZALESKI S. 2010 Drop dynamics after impact on a solid wall: theory and simulations. *Phys. Fluids* **22** (6), 062101.

FUKAI J., ZHAO Z., POULIKAKOS D., MEGARIDIS C.M. & MIYATAKE O. 1993 Modeling of the deformation of a liquid droplet impinging upon a flat surface. *Phys. Fluids A: Fluid Dyn.* **5** (11), 2588–2599.

GARCÍA-GEIJO, P., QUINTERO, E.S., RIBOUX, G. & GORDILLO, J.M. 2021 Spreading and splashing of drops impacting rough substrates. *J. Fluid Mech.* **917**, A50.

GORDILLO, J.M., RIBOUX, G. & QUINTERO, E.S. 2019 A theory on the spreading of impacting droplets. *J. Fluid Mech.* **866**, 298–315.

GORDILLO, L., SUN, T.-P. & CHENG, X. 2018 Dynamics of drop impact on solid surfaces: evolution of impact force and self-similar spreading. *J. Fluid Mech.* **840**, 190–214.

HUANG H.-M. & CHEN X.-P. 2018 Energetic analysis of drop's maximum spreading on solid surface with low impact speed. *Phys. Fluids* **30** (2), 022106.

JHA, A., CHANTELOT, P., CLANET, C. & QUÉRÉ, D. 2020 Viscous bouncing. *Soft Matt.* **16** (31), 7270–7273.

JØRGENSEN, L. 2024 Deformation of drops at low Reynolds number impact. *Phys. Rev. Fluids* **9** (8), 083601.

JOSSERAND, C. & THORODDSEN, S.T. 2016 Drop impact on a solid surface. *Annu. Rev. Fluid Mech.* **48**, 365–391.

KIM, H.-Y. & CHUN, J.-H. 2001 The recoiling of liquid droplets upon collision with solid surfaces. *Phys. Fluids* **13** (3), 643–659.

KUNDU, P.K. & COHEN, I.M. 2002 *Fluid Mechanics*. Elsevier.

LAAN, N., DE BRUIN, K.G., BARTOLO, D., JOSSERAND, C. & BONN, D. 2014 Maximum diameter of impacting liquid droplets. *Phys. Rev. Appl.* **2** (4), 044018.

LAGUBEAU, G., FONTELOS, M.A., JOSSERAND, C., MAUREL, AÈS, PAGNEUX, V. & PETITJEANS, P. 2012 Spreading dynamics of drop impacts. *J. Fluid Mech.* **713**, 50–60.

LEE, J.B., DEROME, D., DOLATABADI, A. & CARMELIET, J. 2016*a* Energy budget of liquid drop impact at maximum spreading: numerical simulations and experiments. *Langmuir* **32** (5), 1279–1288.

LEE, J.B., DEROME, D., GUYER, R. & CARMELIET, J. 2016*b* Modeling the maximum spreading of liquid droplets impacting wetting and nonwetting surfaces. *Langmuir* **32** (5), 1299–1308.

LEE, J.B., LAAN, N., DE BRUIN, K.G., SKANTZARIS, G., SHAHIDZADEH, N., DEROME, D., CARMELIET, J. & BONN, D. 2016c Universal rescaling of drop impact on smooth and rough surfaces. *J. Fluid Mech.* **786**, R4.

LIANG, G., CHEN, Y., CHEN, L. & SHEN, S. 2019 Maximum spreading for liquid drop impacting on solid surface. *Ind. Engng Chem. Res.* **58** (23), 10053–10063.

LIN, S., ZHAO, B., ZOU, S., GUO, J., WEI, Z. & CHEN, L. 2018 Impact of viscous droplets on different wettable surfaces: impact phenomena, the maximum spreading factor, spreading time and post-impact oscillation. *J. Colloid Interface Sci.* **516**, 86–97.

LIU, H.-R., ZHANG, C.-Y., GAO, P., LU, X.-Y. & DING, H. 2018 On the maximal spreading of impacting compound drops. *J. Fluid Mech.* **854**, R6.

LIU, L., CAI, G. & TSAI, P.A. 2020 Drop impact on heated nanostructures. *Langmuir* **36** (34), 10051–10060.

LIU, L., HE, B., WANG, W., CAI, G. & TSAI, P.A. 2023 Ionic liquid drop impact onto heated surfaces. *Phys. Rev. Fluids* **8** (7), 073602.

LIU, L., ZHANG, Y., CAI, G. & TSAI, P.A. 2022 High-speed dynamics and temperature variation during drop impact on a heated surface. *Intl J. Heat Mass Transfer* **189**, 122710.

LOHSE, D. 2022 Fundamental fluid dynamics challenges in inkjet printing. *Annu. Rev. Fluid Mech.* **54**, 349–382.

LOLLA, V.Y., AHMADI, S.F., PARK, H., FUGARO, A.P. & BOREYKO, J.B. 2022 Arrested dynamics of droplet spreading on ice. *Phys. Rev. Lett.* **129** (7), 074502.

MA, X., ALDHALEAI, A., LIU, L. & TSAI, P.A. 2024 Nanofluid drop impact on heated surfaces. *Langmuir* **40** (7), 3640–3650.

MADEJSKI, J. 1976 Solidification of droplets on a cold surface. *Intl J. Heat Mass Transfer* **19** (9), 1009–1013.

MAO, T., KUHN, D.C.S. & TRAN, H. 1997 Spread and rebound of liquid droplets upon impact on flat surfaces. *AIChE J.* **43** (9), 2169–2179.

MARMANIS, H. & THORODDSEN, S.T. 1996 Scaling of the fingering pattern of an impacting drop. *Phys. Fluids* **8** (6), 1344–1346.

MCCARTHY L.P., REID J.P. & WALKER J.S. 2023 High frame-rate imaging of the shape oscillations and spreading dynamics of picolitre droplets impacting on a surface. *Phys. Fluids* **35** (12), 122010.

MONGRUEL, A., DARU, V., FEUILLEBOIS, F. & TABAKOVA, S. 2009 Early post-impact time dynamics of viscous drops onto a solid dry surface. *Phys. Fluids* **21** (3), 032101.

PASANDIDEH-FARD M., QIAO Y.M., CHANDRA S. & MOSTAGHIMI J. 1996 Capillary effects during droplet impact on a solid surface. *Phys. Fluids* **8** (3), 650–659.

PHILIPPI, J., LAGRÉE, P.-Y. & ANTKOWIAK, A. 2016 Drop impact on a solid surface: short-time self-similarity. *J. Fluid Mech.* **795**, 96–135.

PROSPERETTI, A. 1980 Free oscillations of drops and bubbles: the initial-value problem. *J. Fluid Mech.* **100** (2), 333–347.

QUÉRÉ, D. 2013 Leidenfrost dynamics. *Annu. Rev. Fluid Mech.* **45**, 197–215.

RIBOUX, G. & GORDILLO, J.M. 2014 Experiments of drops impacting a smooth solid surface: a model of the critical impact speed for drop splashing. *Phys. Rev. Lett.* **113** (2), 024507.

RIOBOO, R., TROPEA, C. & MARENGO, M. 2001 Outcomes from a drop impact on solid surfaces. *Atomiz. Sprays* **11** (2), 155–165.

ROISMAN I.V. 2009 Inertia dominated drop collisions. II. An analytical solution of the Navier–Stokes equations for a spreading viscous film. *Phys. Fluids* **21** (5), 052104.

SANJAY V. & LOHSE D. 2025 Unifying theory of scaling in drop impact: forces and maximum spreading diameter. *Phys. Rev. Lett.* **134** (10), 104003.

SANJAY, V., ZHANG, B., LV, C. & LOHSE, D. 2025 The role of viscosity on drop impact forces on non-wetting surfaces. *J. Fluid Mech.* **1004**, A6.

SCHELLER, B.L. & BOUSFIELD, D.W. 1995 Newtonian drop impact with a solid surface. *AIChE J.* **41** (6), 1357–1367.

SCHINDELIN, J. *et al.* 2012 Fiji: an open-source platform for biological-image analysis. *Nat. Methods* **9** (7), 676–682.

SCHLICHTING, H. & GERSTEN, K. 2016 *Boundary-Layer Theory*. Springer.

SEN, S., VAIKUNTANATHAN, V. & SIVAKUMAR, D. 2014 Experimental investigation of biofuel drop impact on stainless steel surface. *Expl Therm. Fluid Sci.* **54**, 38–46.

SEO, J., LEE, J.S., KIM, H.Y. & YOON, S.S. 2015 Empirical model for the maximum spreading diameter of low-viscosity droplets on a dry wall. *Expl Therm. Fluid Sci.* **61**, 121–129.

SINGH, R.K., HODGSON, P.D., SEN, N. & DAS, S. 2021 Effect of surface roughness on hydrodynamic characteristics of an impinging droplet. *Langmuir* **37** (10), 3038–3048.

SNOEIJER, J.H. & ANDREOTTI, B. 2013 Moving contact lines: scales, regimes, and dynamical transitions. *Annu. Rev. Fluid Mech.* **45** (1), 269–292.

SOTO, D., DE LARIVIÈRE, A.B., BOUTILLON, X., CLANET, C. & QUÉRÉ, D. 2014 The force of impacting rain. *Soft Matt.* **10** (27), 4929–4934.

TANG, C., QIN, M., WENG, X., ZHANG, X., ZHANG, P., LI, J. & HUANG, Z. 2017 Dynamics of droplet impact on solid surface with different roughness. *Intl J. Multiphase Flow* **96**, 56–69.

THORODDSEN, S.T., TAKEHARA, K. & ETOH, T.G. 2012 Micro-splashing by drop impacts. *J. Fluid Mech.* **706**, 560–570.

TONINI, S. & COSSALI, G.E. 2024 Analytical model of small-and large-amplitude drop oscillation dynamics. *Phys. Fluids* **36** (11), 117147.

TSAI, P., HENDRIX, M.H.W., DIJKSTRA, R.R.M., SHUI, L. & LOHSE, D. 2011 Microscopic structure influencing macroscopic splash at high Weber number. *Soft Matter* **7** (24), 11325–11333.

TSAI, P., PACHECO, S., PIRAT, C., LEFFERTS, L. & LOHSE, D. 2009 Drop impact upon micro-and nanostructured superhydrophobic surfaces. *Langmuir* **25** (20), 12293–12298.

TSAI, P., C. A. VAN DER VEEN, R., VAN DE RAA, M. & LOHSE, D. 2010 How micropatterns and air pressure affect splashing on surfaces. *Langmuir* **26** (20), 16090–16095.

UKIWE, C. & KWOK, D.Y. 2005 On the maximum spreading diameter of impacting droplets on well-prepared solid surfaces. *Langmuir* **21** (2), 666–673.

WANG R., SHI Y.-Z., ZHANG C.-Y. & DING H. 2022*a* On the maximal spreading of drops impacting onto a no-slip substrate. *Phys. Fluids* **34** (5), 052103.

WANG, Y., AMBERG, G. & CARLSON, A. 2017 Local dissipation limits the dynamics of impacting droplets on smooth and rough substrates. *Phys. Rev. Fluids* **2** (3), 033602.

WANG, Y.-F., WANG, Y.-B., HE, X., ZHANG, B.-X., YANG, Y.-R., WANG, X.-D. & LEE, D.-J. 2022b Scaling laws of the maximum spreading factor for impact of nanodroplets on solid surfaces. *J. Fluid Mech.* **937**, A12.

WILDEMAN, S., VISSER, C.W., SUN, C. & LOHSE, D. 2016 On the spreading of impacting drops. *J. Fluid Mech.* **805**, 636–655.

YARIN, A.L. 2006 Drop impact dynamics: splashing, spreading, receding, bouncing. *Annu. Rev. Fluid Mech.* **38** (1), 159–192.

YONEMOTO, Y. & KUNUGI, T. 2017 Analytical consideration of liquid droplet impingement on solid surfaces. *Sci. Rep.* **7** (1), 2362.

YUE P. & FENG J.J. 2011 Wall energy relaxation in the Cahn–Hilliard model for moving contact lines. *Phys. Fluids* **23** (1), 012106.

ZHANG, B., SANJAY, V., SHI, S., ZHAO, Y., LV, C., FENG, X.-Q. & LOHSE, D. 2022 Impact forces of water drops falling on superhydrophobic surfaces. *Phys. Rev. Lett.* **129** (10), 104501.